Results in Engineering 25 (2025) 104251

Contents lists available at ScienceDirect

Results in Engineering

journal homepage: www.sciencedirect.com/journal/results-in-engineering

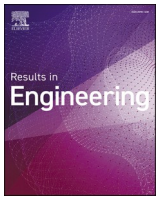

Research paper

Effect of plasma assisted combustion on emissions of a premixed nitrous oxide fuel blend☆

Boj N. Villanueva [a], Po-Hung Lin [b], Yueh-Heng Li [b,c,*], Jaime P. Honra [a]

[a] School of Mechanical, Manufacturing, and Energy Engineering, Mapua University, Manila, Metro Manila, Philippines
[b] Department of Aeronautics and Astronautics, National Cheng Kung University, Tainan, 70101, Taiwan
[c] Institute of Space Systems Engineering, National Cheng Kung University, Tainan, 70101, Taiwan

ARTICLE INFO

Keywords:
Nitrous Oxide Fuel Blend (NOFBX)
Plasma assisted combustion
NO_x emissions
Chemiluminescence

ABSTRACT

Hydrocarbon/Nitrous Oxide fuel blends, commonly called HyNOx or NOFBX, are currently being researched for aeronautic and aerospace propellant applications due to its good performance and economy. However, research on the fuel blend is relatively scant, especially regarding its emission characteristics, as the composition may produce high NO_x emissions, which are harmful to both human society and the environment. This study sought to utilize Nanosecond Pulsed Dielectric Barrier Discharge plasma as an emission control mechanism as not only has it found success as a pollution control mechanism, but also as a combustion enhancement one. Chemiluminescence imaging was used to observe the changes in radical species emissions for a laminar premixed CH_4/N_2O/Ar flame under plasma actuation and emission results were measured with a flue gas analyzer. It was found that once the input voltage crossed a critical value, the chemiluminescent concentrations of CH* and NH_2* saw a significant rise, leading non-monotonic increase in the concentration of NOx with this phenomenon lessening as equivalence ratios increased, with the stoichiometric emissions being relatively unaffected. This occurrence was speculated to be from the plasma promotion of the Prompt NO pathway in lean conditions, which was supported by greatly increased OH* radical concentrations. Other emissions such as the Unburned Hydrocarbon CH_4 and CO_2 were found to decrease non-monotonically with increasing plasma intensity after the input voltage crossed the critical value, with the result being a product of various plasma combustion enhancement mechanisms such as dissociation and excitation.

1. Introduction

Despite its long heritage, good performance, and long term stability, there is a serious effort being pushed toward replacing the common propulsion monopropellant Hydrazine (N_2H_4) for use in military and aviation applications [1]. This is in part due to its extreme toxicity, as even workers conducting routine maintenance near these products have been exposure to levels above and beyond standard exposure limits, causing injury to the lungs and other small tissue, as well as seizures, comas, and in the worst case scenario, loss of life [2]. Possible alternatives currently being studied include propellants whose primary components include hydrogen peroxide, nitrous oxide, and ammonia-based blends [3,4]. Outside of these, the mixture of a hydrocarbon fuel and a nitrous oxide oxidizer, known as $HyNO_x$ (Hydrocarbons and Nitrous Oxide) or NOFBX, is also one such candidate. Nitrous Oxide alone possesses low thermal sensitivity and performance, which necessitates the blending of hydrocarbon fuels such as Methane (CH_4) or Ethylene (C_2H_4) [5–7].

Previous research on this particular fuel blend has yielded promising results, such as a higher specific impulse and accessible storage in the liquid phase, which allows for easier transport and availability, compared to Hydrazine which requires more specialized processing [8]. This also contributes to the overall lower costs associated, which come about from NOFBX being nontoxic and having a large applicability range, further increasing its potential for promising and continued use when it comes to aerospace applications [9]. However, all is not yet well for NOFBX as one neglected aspect of NOFBX is its emission characteristics. Pollutants such as soot, unburned hydrocarbons and sulfides, and

☆ This study considers only original articles that have not been published elsewhere and are not currently under consideration by another journal published by Wiley or any other publisher.

* Corresponding author at: Department of Aeronautics and Astronautics, National Cheng Kung Univ., Tainan, 70101, Taiwan.
E-mail address: yueheng@mail.ncku.edu.tw (Y.-H. Li).

https://doi.org/10.1016/j.rineng.2025.104251
Received 13 November 2024; Received in revised form 16 January 2025; Accepted 2 February 2025
Available online 3 February 2025

especially NOx are just some of the products formed during the combustion of Hydrocarbon and Nitrous Oxide mixtures [10] Emission of these Nitrogen Oxides (NO and NO_2) are a major contributor when it comes to air pollution, as they contribute to the formation of smog and acid rain, which are not only harmful to the environment, but also to human health [11].

While there has already been a good amount of research done when it comes to NOx abatement in combustion applications, such as through chemical scrubbing [12], adsorption, or catalytic reduction [13], these measures alone are insufficient to deal with the ever-increasing strictness of government regulations and ever-growing demand for industrialization in a world that grows more interconnected every day. Therefore, not only are improvements to existing methods important, but also new emission control technologies must be developed. One such development making significant headway when it comes to combustion and aerospace applications is the use of Plasma Assisted Combustion (PAC), in part due to the characteristics of plasma such as low energy consumption and easy control being in-line with combustion advancement [14] .

1.1. State of the problem and recent advances

PAC has been rapidly gaining interest due to its potential for great improvements when it comes to the combustion process. Generated by inducing electrical breakdown into a gas, PAC has been found as an effective method to improve the performance of combustion processes [15]. Primarily making use of Non-Equilibrium Plasma, the generated high–energy electron and ion mixture interact with the fuel, producing various active and intermediate species which aid in the flammability process through the kinetic, transport, and thermal pathways [16]. These pathways have been found to enhance the unburnt gas and the fuel; oxidation process, improving the parameters of the combustion process and overall flammability [17].

Plasma has seen use in several model combustion applications, such as in one investigation conducted by Tian et al. [18], wherein even the most basic of AC arc plasma was able to induce significant combustion enhancements in a model scramjet. They made use of CH* chemiluminescence to explain the plasma-induced phenomenon such as increased static pressure and flame intensity, showcasing its usefulness for combustion applications. Sun et al. [19] investigated the stabilizing effects of non-thermal plasma on the combustion reaction and discovered this could also improve the operational range capacity of the combustion reaction by extending the lean flammability limit. PAC has also been found to reduce both the necessary time and temperature for combustion. Tang et al. [20] managed to reduce the ignition temperature for a methane-oxygen counterflow diffusion flame by almost 200 K, in addition to extending the extinction limit by approximately 20 %. Their use of Planar Laser-Induced Fluorescence (PLIF) revealed a substantial increase in the signal reception of the methylidyne radical, which agreed with the previous literature on the combustion enhancement pathways of PAC, the production of active species, radicals, and additional stable molecules. Non-thermal plasma in combustion reactions are capable of functioning as emission control mechanisms by various means, and as such are able to act as an alternative technology for DeNOX solutions. Plasma has also been shown to possess the ability to greatly stabilize the combustion process, as reported in a paper by Feng et al. wherein gliding arc plasma was used to suppress combustion transition in scramjet [21]. Through the use of OH* chemiluminescence alongside other diagnostic tools, they were able to suppress the oscillation of the flame in the scramjet combustor, up to above 90 % stability mode. Through the chemiluminescence, their plausible explanation involved the increased reactions due to the induced N_{2^*} and O generated by plasma, which enhanced the oxidation effect in its vicinity, promoting temperature rise and better mixing. Molchanov et al. [22] made use of electrostatic precipitators to generate DC voltage in the hopes of reducing both particulate matter and NOx for a study, alongside the development of a kinetic model for predictions. Their findings reveal significant implications for the future of PAC in emission reduction technologies, particularly for biomass systems, as a significant amount of NOx was reduced with almost 99 % particulate matter removal efficiency, building a foundation for better control mechanisms in the future.

Recent works have also considered the effects of PAC for emission controls, which serve to justify the grounds of this study as in-line with the most cutting edge developments in plasma use for combustion applications. . In 2023, Ju et al. [23] used gliding arc plasma in a swirl combustor to influence the characteristics of an ammonia/air flame. Their results showed that in certain conditions, it was possible to reduce emissions by almost 21 % and this was mainly attributed to the ability of plasma as a fuel cracking mechanism, facilitating the consumption of NO by the disassociation of ammonia. Another study involving PAC as an emission control mechanism was done by Paulauskas et al. [24] using a flat flame burner and dielectric barrier discharge (DBD) actuator. They sought to use the ozone generated by plasma in order to bolster the consumption of biogas with varying CO2 content and chemiluminescence on OH* and CH* was used to analyze the overall flame characteristics. It was found that the presence of plasma increased the presence of said radicals due to the elevated levels of oxygen as a result of the decomposition of ozone generated by the plasma. Additionally, both CO and NOx emissions in the presence of plasma were discovered to be lower than in the absence, with the reduction in CO being as high as 40 %. These developments show the great amount of potential plasma application has, despite being the body of knowledge regarding its specific interactions with the combustion process being relatively scant.

1.2. Current limitations and research gap

Regardless of these advances, there remains a great deal of work to be accomplished when it comes to taking plasma applications into mainstream combustion applications. Li et al. [25] discusses in a review of plasma applications for aerospace combustors highlights the lack of understanding between the coupling of the flame and plasma regimes, which is theorized to influence several important parameters such as the energy efficiency of the system and the overall combustion enhancement effect of the plasma system. Their paper suggests further inquiry towards both the combustion mechanics and the physical interacts of plasma assistance, which points necessitates further research towards plasma-flame interactions, in the hopes of achieving reliable and stable combustion of engines under the extreme conditions required. The effect of PAC on emissions was also considered in their study, calling attention to the more stringent environmental regulations and novel low-emission combustors, both of which could be served by plasma assistance.

Building off the concern of environmental regulations, the initially proposed NOFBX has had little in the way in terms of dedicated and detailed investigation towards its emission characteristics. The decomposition of Nitrous Oxide in the fuel results in an oxygen-rich environment and highly exothermic temperature release, which may promote the formation of NOx, a hazard to both humans and the environment [26]. While there have been several mentions of NOx abatement technologies already mentioned in this study, as of the time of writing this paper, those techniques have yet to be applied towards NOFBX fuels, especially PAC. While there already exists research on PAC for NOx reduction, such as one by Ju et al. [27], where it was found that Gliding Arc (GA) plasma was able to reduce the NOx emissions of an Ammonia/air mixture, these results cannot be generalized towards the wide spectrum of combustion fuels as a whole, and as such it becomes a paramount endeavor to see if the emission control aspect is able to extend to various kinds, especially one such as NOFBX which is under development as a “green propellant” for spacecraft and orbital propulsion applications [28].

1.3. Objectives and novelty of the study

For the purposes of this study, a nanosecond-pulsed Dielectric Barrier Discharge (ns-DBD) system is used to generate the non-thermal plasma in the hopes of reducing the NOx emissions of the NOFBX mixture, which is composed of Nitrous Oxide (N_2O) and Methane (CH_4). The ns-DBD system is used as not only is there is a comprehensive body of research on its combustion enhancement effects, but also the ease of access it can be set up [29]. This allows for a simplified PAC system wherein the combustible mixture travels upstream from the gas tanks towards the plasma area before exiting the slot burner. The intensity of the plasma system is then modified by adjusting the input voltage of the nanosecond pulse generator, which may allow a trend or pattern to be observed with changing energy levels. Additionally, chemiluminescence imaging of key combustion radicals, namely OH* (Hydroxyl), CH* (Methylidyne), and NH_2* (Amino) is used on the flame front in order to better understand how PAC affects the changes in the chemical composition of the burning flame and how it `fluctuates with the emission concentration readings. Chemiluminescence has been a significant tool in the field of flame characterization due to its simple, non-intrusive, and economic properties, especially when it comes to investigating the intermediate chemical reactions and drawing analyses from the recorded concentrations, such as in one such study by Sun et al. [30] regarding Ammonia/Methane/Air flames and GA plasma.

By using both chemiluminescence and recording of emission changes due to plasma excitation through a flue gas analyzer, a better understanding of how ns-DBD plasma interacts with Hydrocarbon and Nitrous Oxide fuels can be reached, which contributes to the body of knowledge oof plasma-fuel interactions, diving future researchers to investigate more deeply the complex kinetics between the two phenomena.

The novelty of the study can be found in the first part, as the systematic investigation of using PAC as an emission control mechanism for an NOFBX fuel is supplemented by using the simple and accessible technology of chemiluminescence imagine to explain the changes in particle concentration brought upon by plasma excitation. By combining chemiluminescence imaging of radical species with flue gas analysis, the study provides a novel framework for understanding the interplay between plasma-induced radicals and NOx formation, alongside other pollutant particles such as CO_2 and CH_4. This investigation offers insights to optimize plasma-assisted emission control strategies for sustainable propulsion technology.

2. Theoretical background

2.1. Chemiluminescence and NOx formation pathways

Chemiluminescence makes use of the light emitted from excited state-radicals generated from chemical reactions as they return to the ground state. When it comes to hydrocarbon flames, it can provide useful insights towards the reaction zones [31], equivalence ratios [32], and heat release rate [33] among others. This study hopes that NOx emission trends under plasma effect may also be sensed or represented either by chemiluminescence of single radical species, or ratios thereof. As previously discussed`, this study makes use of OH*, CH*, and NH_2* radicals for the analysis of PAC effects on the emission of NOx and other pollutants, due to their prominence in the investigation and analysis of hydrocarbon flames [34].

The OH* radical is commonly understood to be formed and depleted by the following elementary reactions, [35]

$$H + O + M \leftrightarrow OH^* + M \quad \text{(R1)}$$

$$OH^* \leftrightarrow OH + h\nu \quad \text{(R2)}$$

where M is a third body species. This reaction also highlights the direct proportionality between excited-state OH (OH*) and ground state OH. OH* has been used extensively in chemiluminescence as a diagnostic tool for spatial analysis of heat release zones and other combustion properties such as flame fronts. Ground state OH on the other hand, takes an important part in the Thermal NO or Zeldovich Mechanism, a major source of Nitric Oxide in high temperature combustion processes [36],

$$O + N_2 \leftrightarrow NO + N \quad \text{(R3)}$$

$$N + OH \leftrightarrow NO + H \quad \text{(R4)}$$

$$N + O_2 \leftrightarrow NO + O \quad \text{(R5)}$$

which may indicate a link between OH* and NO_x emissions.

On the other hand, the CH* radical is formed by the reaction between hydrocarbon intermediates with oxygen, as seen below [37]

$$C_2H + O_2 \leftrightarrow CO_2 + CH^* \quad \text{(R6)}$$

$$C_2H + O \leftrightarrow CO + CH^* \quad \text{(R7)}$$

$$CH^* \rightarrow CH + h\nu \quad \text{(R8)}$$

where, similar to the previous radical discussed, direct proportionality exists between the excited stated and the ground state radical. After which during hydrocarbon combustion, ground state CH participates instead in the Prompt NO formation pathway, highlighted by the attack of CH_n radical species on N_2.

$$CH + N_2 \leftrightarrow NCN + H \quad \text{(R9)}$$

$$NCN + H \leftrightarrow HCN + N \quad \text{(R10)}$$

$$HCN + O \leftrightarrow NCO + H \quad \text{(R11)}$$

$$NCO + H \leftrightarrow NH + CO \quad \text{(R12)}$$

$$NH + H \leftrightarrow N + H_2 \quad \text{(R13)}$$

$$N + OH \leftrightarrow NO + H \quad \text{(R14)}$$

This NO formation pathway is especially prevalent when it comes to hydrocarbon/air diffusion flame combustion [36], with the most favorable conditions for this pathway being in the stoichiometric and fuel-rich conditions. The main way this pathway works is through the fixation of molecular nitrogen and the conversion between fixed nitrogen species, and a majority of the comprehensive data on this formation pathway was taken from premixed laminar flames due to their reliability.

The last radical specie observed using its chemiluminescence is NH_2*, which unlike the previous radicals which are involved in the formation of NO, NH_2* is instead involved in the consumption of NO through the Thermal DeNOx mechanism, or selective NO reduction without a catalyst [38]. Ground-state NH_2, which is directly proportional to its excited state counterpart [30], forms from the oxidation of NH_3 and participates in Thermal DeNOx through the following reaction chains involving free radicals.

$$NO + H_2 \leftrightarrow NH_3 + H_2O \quad \text{(R15)}$$

$$NH_3 + H \leftrightarrow NH_2 + H_2 \quad \text{(R16)}$$

$$NH_2 + NO \leftrightarrow NNH + OH \quad \text{(R17)}$$

$$NH_2 + NO \leftrightarrow N_2 + H_2O \quad \text{(R18)}$$

$$NH_2 + NO_2 \leftrightarrow N_2O + H_2O \quad \text{(R19)}$$

$$NH_2 + NO_2 \leftrightarrow H_2NO + NO \quad \text{(R20)}$$

Ammonia present in the hydrocarbon combustion process functions primarily as a reducing agent and its reaction products aid towards the consumption of NO and NO_2, such that any increase in the signal concentration of the NH_2* radical may signal an overall decrease in NO_x emissions.

3. Experimental methodology

3.1. Experimental setup

The laminar slot burner and ns-DBD actuator setup are shown in Fig. 1. The burner contains a quartz slot that measure 60 mm tall, 42 mm wide, and with 1 mm thick walls. The flame exit area comes around to 40 mm x 2mm. Copper plates measuring 10 mm tall were attached at opposite sides if the quartz slot using a ceramic adhesive at distance of 7.5 mm from the burner exit, serving as the high voltage and grounded electrodes. Once power is supplied to the system, the ns-DBD plasma forms in the space inside of the quartz slot. Once the gases arrive at the quartz slot they are activated by the ns-DBD and ignited at the burner exit to form the premixed laminar flame. For the purposes of this study, OH*, CH*, and NH2* chemiluminescent markers were used alongside an Excelitas pco.pixelfly 1.4 USB ICCD camera and the pco.camware computer program. In order to accurately capture the intensity signals of these radicals, a matching band-pass filter was used to isolate the respective signals of each measured species. OH* and NH2* signals were captured around the 310 nm and 632 nm wavelengths respectively using Edmund Optics 10 nm FWHM, 50 mm Mounted Interference Filters while the CH* was recorded with an Andover Corporation Standard Bandpass Optical 50 mm Filter at 430nm.

Table 1 presents the volumetric flow rates of the fuel, oxidizer and the co-flow gas used. To further explore the plasma phenomenon on a hydrocarbon/N2O blend, three different cases investigated: Case I being at stoichiometric condition (ϕ=1.0); Case II at slightly fuel-lean condition (ϕ=0.8); and Case III at fuel-lean condition (ϕ=0.6), where ϕ is calculated from

Table 1
Flow rates of the fuel, oxidizer, and co-flow gas under different ϕ values.

	Fuel	Oxidizer	Co-Flow
	CH_4	N_2O	Ar
	L/min	L/min	L/min
$\phi = 1.0$	1.54	6.17	3.32
$\phi = 0.8$	1.27	6.35	3.42
$\phi = 0.6$	0.98	6.53	3.52

$$\phi = \frac{\left(\frac{A}{F}\right)_{stoichiometric}}{\left(\frac{A}{F}\right)} = \frac{\left(\frac{m_{air}}{m_{fuel}}\right)_{stoichiometric}}{\left(\frac{m_{air}}{m_{fuel}}\right)} \quad (1)$$

Unfortunately, due to safety concerns regarding the risk of NOFBX flame flashback damaging the quartz slot, fuel-rich conditions were deferred for future studies. Argon was used as the co-flow gas to pair the combustible mixture, as it is often used in PAC studies as a diluent [39]

The fuel and the oxidizer were supplied via high-pressure gas cylinders, with the pressure regulated at 2–3 bar through pressure regulators. Volumetric flow rates were adjusted with Brooks Instrument 5850E Thermal Mass Flow Controllers and calibrated with a MesaLabs' Bios DryCal Definer 220 gas flow calibrator. The flow readings themselves were observed through a PROTEC Instruments PC-540 MFC Readout Power Supply. Initial temperatures of all inlet gases were 25 °C or room temperature.

The power source used to generate the ns-DBD plasma was an FID GMBH Nanosecond Pulse Generator (Model FPG 10–50NM10), which generated a DC signal. The operating frequency ranged from 10 – 40 kHz, while the output voltage of the power supply measured up to 10 kV at maximum amplitude. The voltage applied to the electrodes were changed by adjusting this voltage input. From the power supply, two leads which carried a positive and negative voltage pulse respectively were connected to the electrode. Voltage and frequency profiles from the pulse generated were measured with a high voltage probe Pintek High Voltage Probe (15-HF) while current was evaluated through a Pearson Electronics Wide Band Current Monitor Model 301X Rogowski

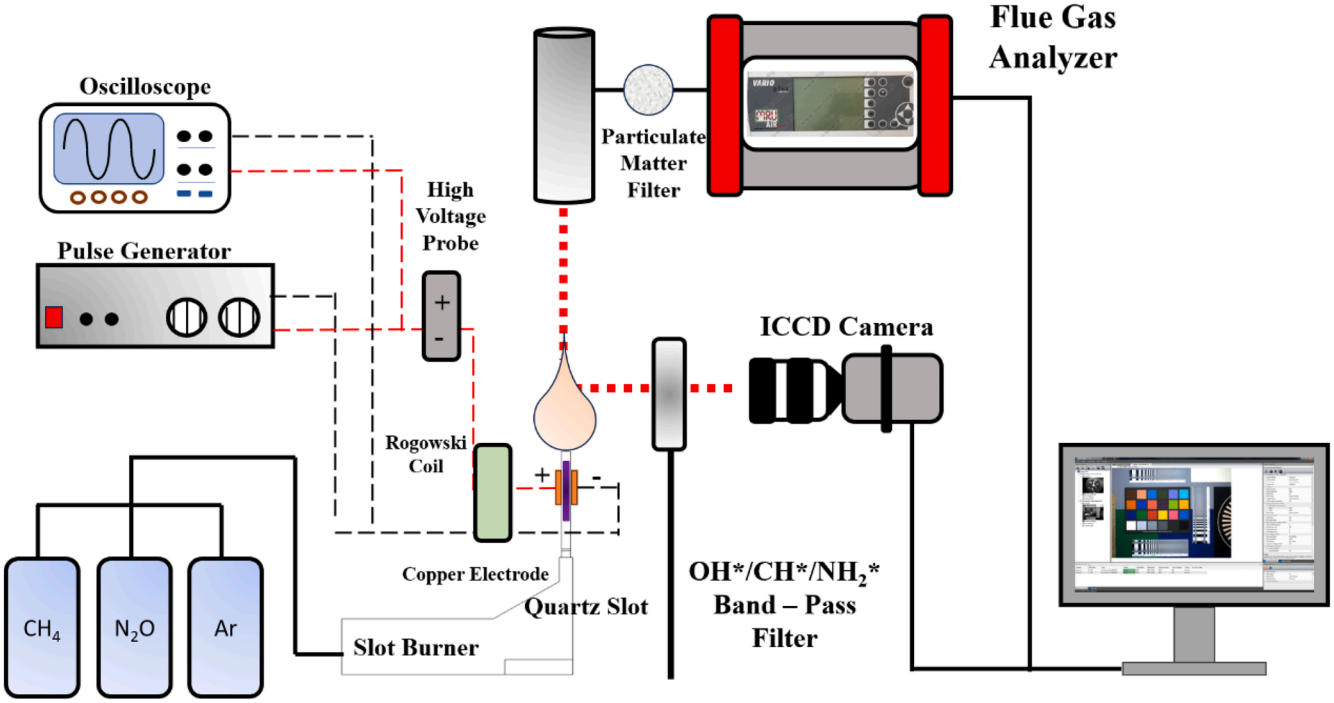

Fig. 1. Experimental Setup.

Coil. These readings were then recorded through a Teledyne Lecroy Wavesurfer 4024 High Definition Oscilloscope. Direct images of the flame and discharge morphology were captured with a Fujifilm X – H2 Camera.

In order to characterize the level of plasma intensity, the Root Mean Square (RMS) Voltage was used. Based on a previous study conducted by Varella et al. [40] which involved gliding arc plasma and a flame of natural gas and air, the RMS of a signal, or in the case of this study, a pulse, is the root of the average of the square of the instantaneous values, often used in signal processing applications. The RMS voltage is given by

$$V_{RMS} = \sqrt{\frac{1}{T}\int_0^T V(t)^2 dt} \quad (2)$$

where T represents the time interval and V(t) corresponds to the voltage as captured in the oscilloscope.

The voltage and power waveforms of the DBD plasma is shown in Fig. 2 for a single pulse, with the input voltage of Fig.2(a) being set to the minimum value of 2.5 kV and Fig. 2(b) at the maximum of 10kV. Both are set to a pulse frequency of 10 kHz. Additionally, the shape of the purple plasma appears to change with the medium, as seen in Fig. 3(a) with Argon and Fig. 3(b) in dry air, the former showing more perpendicular streamers individual and the latter a more homogenous parallel striation. The difference between the two appearances of ns-DBD plasma aligns with the description of Ebrahimi et al. [41] regarding dielectric plasma regimes.

The experimental data gathering sequence was conducted at standard sea level values for pressure and temperature, under the

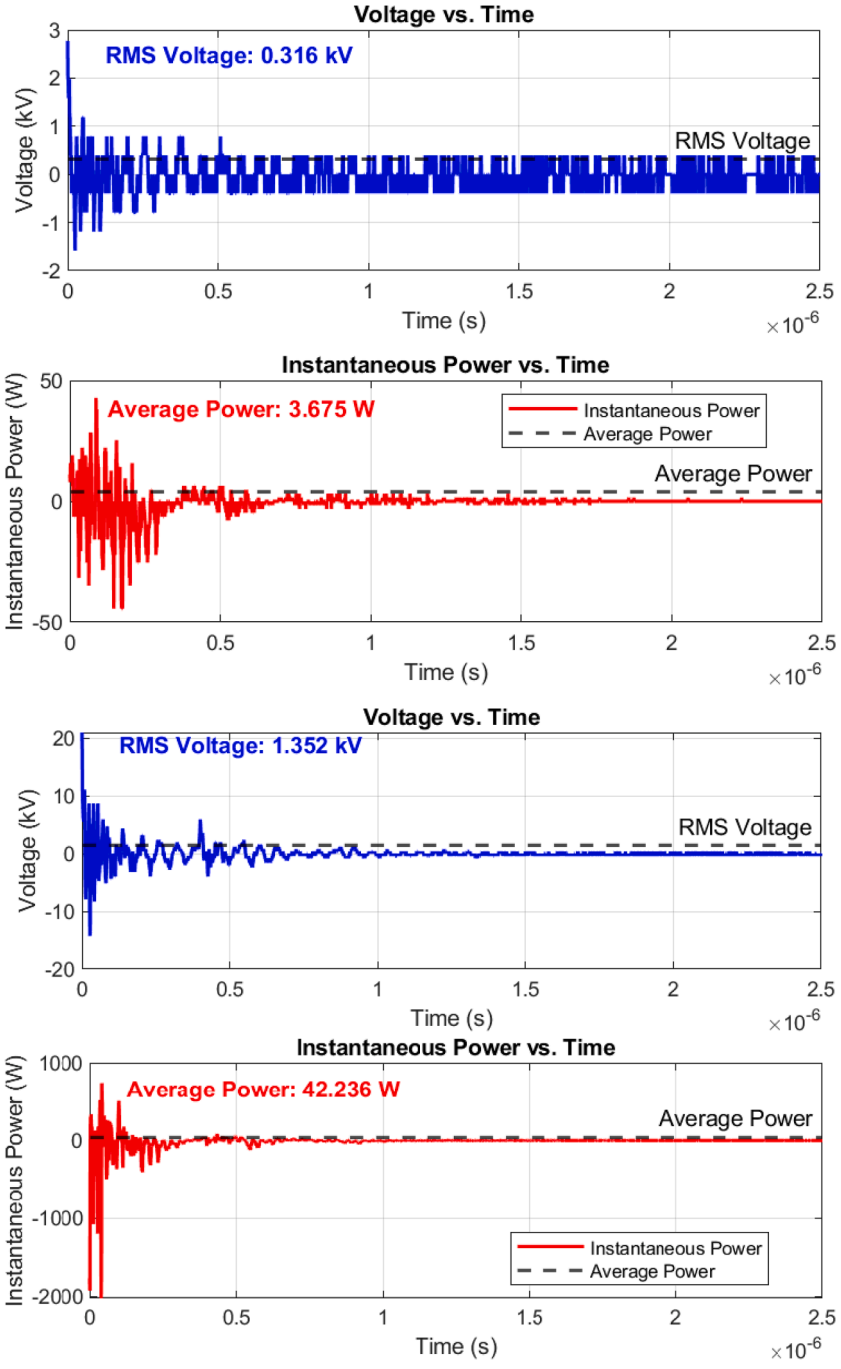

Fig. 2. (a) Voltage-Power Waveform at 2.5 kV Input Voltage. Fig. 2(b) Voltage-Power Waveform at 10 kV Input Voltage.

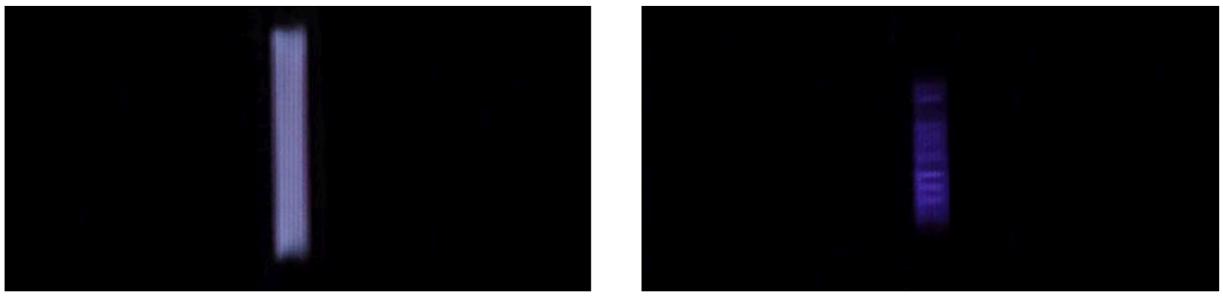

Fig. 3. Direct image of the ns-DBD plasma in: **(a)** Argon and **(b)** Dry Air.

assumption that for the purposes of the current study, environmental conditions were of negligible concern when it came to affecting the recorded data values for emission concentrations and chemiluminescence signals.

3.2. Experimental process

To properly quantify the effect of the ns-DBD plasma on the Hydrocarbon/N2O fuel, it was necessary to measure the concentration of the flue gases produced during the combustion process, namely CH4, CO, CO2, and NOx (NO and NO2). An MRU Instruments VARIO PLUS Portable Syngas Analyzer was used as the monitoring system for the flue gas. When it comes to the measurement method, the values for pollutant emission were recorded per second as the combustion reaction was ongoing through a gas monitoring system. The values were observed on the MRU OnlineView Version 2.9.9 program through a laptop attached to the flue gas analysis device. Values were recorded for 2 min after both the flame and the emission trends stabilized, resulting in 120 data points per case, and the average value taken as the result. Probe location was fixed at a height around 15 cm above the flame tip. Based on its user manual, the flue gas analyzer possesses a detection limit of around 0.05 % or around 1 ppm with regards to the recorded concentration readings.

The control sequence of the experiment begins with setting the flowmeter values to the designated level for the current equivalent ratio, starting with the lowest at $\phi = 0.6$, increasing until stoichiometric conditions. Once the values have been set, the flow controllers are activated and the flame is ignited. The NOFBX flame is allowed to burn for 2–3 min to stabilize before chemiluminescence images are taken. Once the images have been taken for the No Plasma (NP) condition, the pulse generator is turned on and set to the minimum conditions, Once again, the flame is left to burn for a few minutes under the new condition, allowing the readings of the gas analyzer to stabilize, then the chemiluminescence images are taken. After the images have been recorded, the pulse generator is returned to the lowest setting and the process repeats for each level of input voltage and frequency. Once the maximum values of voltage and frequency have had their chemiluminescence images taken and flue gases analyzed, the burner system is turned off and purged with air for a few minutes before the next level of equivalence ratio is investigated.

3.3. Quality control and data normalization

In order to ensure that the chemiluminescence images for the recorded radicals are free from interference, the following steps were taken based on the work done by Liu et al. [42] in their study of OH* and CH* radicals in a swirl flame. Before any chemiluminescence could take place, background signals were recorded. Then, during the image taking process proper, 100 images overall were taken and averaged. The averaged images then had the background signals subtracted and had a Gaussian smoothing filter applied. Lastly, the images were normalized to the maximum values recorded and were cropped to focus solely on the flame cone area, the immediate space above the burner exit formed from a delicate balance of flame propagation speed and unburned mixture velocity, which may yet be affected by plasma exciation. This was done to concentrate and focus the analysis on the immediate combustion processes occurring near and around the burner exit.

To account for emission standards [43], the measured values were adjusted to 15 % O_2 and henceforth shall be referred to as relative emissions to avoid confusion. How the emission values were normalized to these standards is given by the correction factor equation

$$c_f = \frac{21 - \%O_2^{ref}}{21 - \%O_2^{exh}} \tag{3}$$

wherein c_f stands for the correction factor, $\%O_2^{ref}$ corresponds to the reference O_2vol fraction and $\%O_2^{exh}$ means the exhaust O_2vol fraction. Additionally, since both CO and CO_2 concentrations are able to be recorded by the flue gas analyzer, the combustion efficiency before and after plasma effects can also be defined [44] as follows:

$$\eta_e = \frac{CO_2}{CO_2 + CO}\ x\ 100\% \tag{4}$$

wherein η_e refers to the overall combustion efficiency as a ratio of the partially burned carbon, CO, and the fully burned carbon, CO_2. CO_2 and CO refer to their dry volume concentrations in parts per million.

4. Results and discussion

4.1. Chemiluminescent images and radical concentrations

Fig. 6 shows the direct image chemiluminescent signal intensities of the OH*, CH*, and NH_2* species found in the of the premixed laminar CH_4/N_2O/Ar flame. For the purposes of this study, the half-images of chemiluminescent signals taken from the left or electrode side will be taken as symmetric for the whole flame. Additionally, it can be seen that the inner flame cone decreases in height as ϕ increases, which, for laminar flames, represents an increase in burning velocity [17] as shown in the following equation,

$$S_L = U_o \sin\alpha \tag{5}$$

wherein S_L represents the laminar burning velocity, U_0 is the unburned gas velocity, and α represents the semi-cone angle of the flame cone. The inner flame cone is a representation of one of the most important parameters when it comes to combustible mixtures: the laminar burning velocity [45]. Generally speaking it is understood as a conical shape that forms due to the balance of velocities between the flame propagation and the unburned gas mixture. It can be seen that as the decrease of height in the inner flame cone is difficult to observe from the images alone, the chemiluminescent signal intensities at a 1.5 mm above the burner exit, or halfway above the flame cone, were taken in order to better understand the effect of ns-DBD on flame shape. These are shown in Fig. 5. These readings were taken from the outer region of the flame going inwards, under different equivalence ratios and in the presence

and absence of plasma excitation.

It can be seen that, across all recorded species, peak signal intensity is recorded at stoichiometric conditions and in the presence of ns-DBD plasma, which shows that a local increase in their concentrations has been observed compared to the absence of plasma, at least when it comes to the flame cone. Since the drop in radical signal intensity is shifts further right with increasing plasma power, this could also be taken to mean that the flame cone height is reduced, therefore highlighting the ability of ns-DBD plasma to influence the laminar burning velocity, which agrees with prior literature [46], however as this observation was only made qualitatively through image analysis, further work is required to properly systematize this phenomenon.

Previous research done [19] has shown the ability of PAC to stabilize flames and the chemiluminescent results appear to be in good agreement. Additionally, the increase in radical species may be attributed to the increase in molecular Oxygen from the reduction of Ozone generated by plasma [47] in reactions with N2O and O2 as seen below

$$N_2O + O \leftrightarrow N_2 + O_2 \quad \text{(R21)}$$

$$N_2^* + O_2 \leftrightarrow N_2 + 2O \quad \text{(R22)}$$

$$O_2 + e \leftrightarrow O + O + e \quad \text{(R23)}$$

$$O_2 + O + M \leftrightarrow O_3 + M \quad \text{(R24)}$$

$$O_3 + O \rightarrow 2O_2 \quad \text{(R25)}$$

wherein the increased amount of O_2 formed in R25 leads to an increased amount of OH* and CH* through R1 and R6 respectively.

Observing the spatial concentrations of the species themselves in Fig. 4, it can be seen that while the concentrated chemiluminescence images of the OH* radical remain consistent before and after plasma

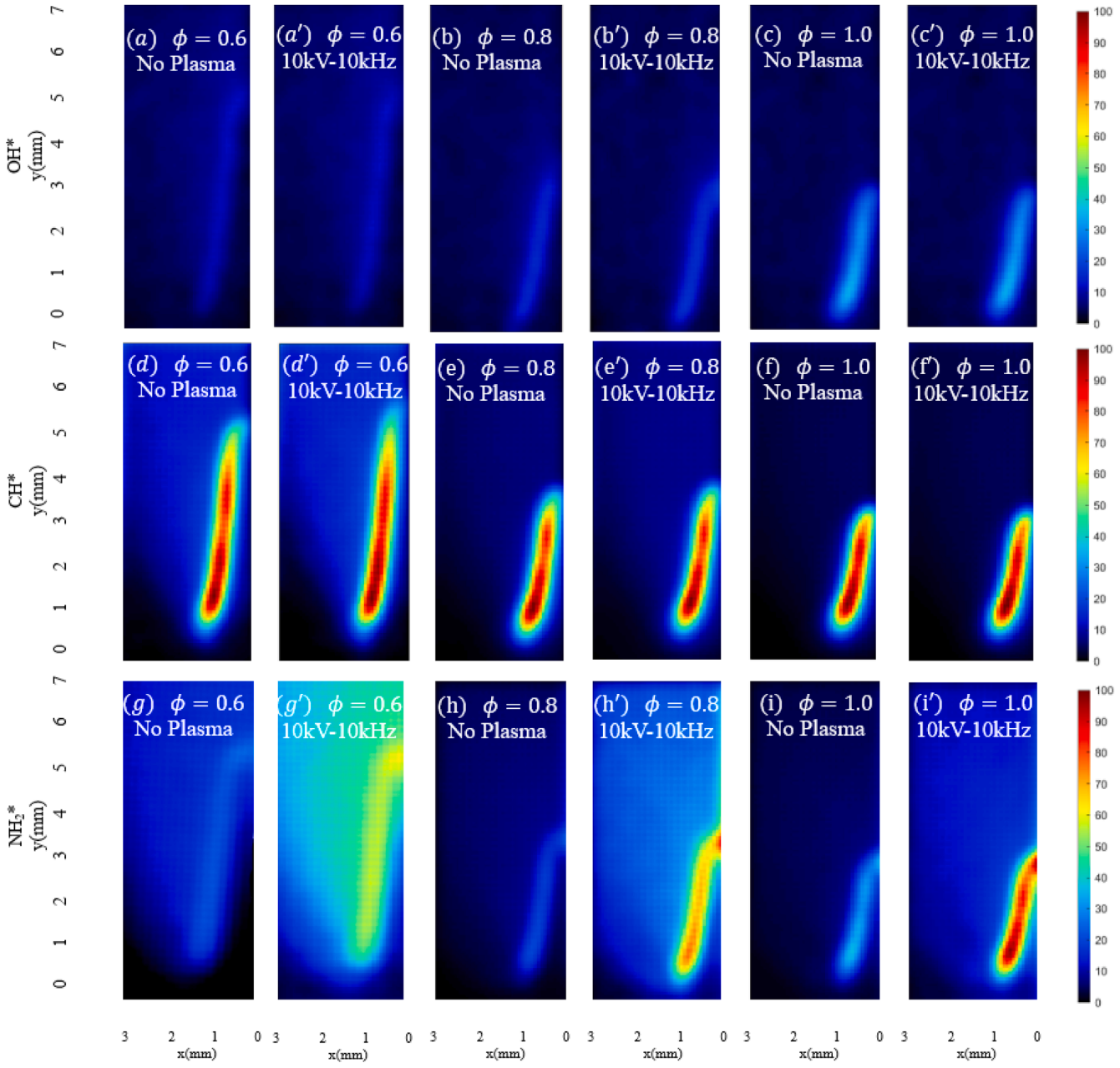

Fig. 4. . Chemiluminescent images at the area surrounding the flame cone of different radicals species present in the $CH_4/N_2O/Ar$ flame at different values of ϕ in the absence (a)-(i) and presence of Nanosecond Pulsed Dielectric Barrier Discharge plasma (a')-(i').

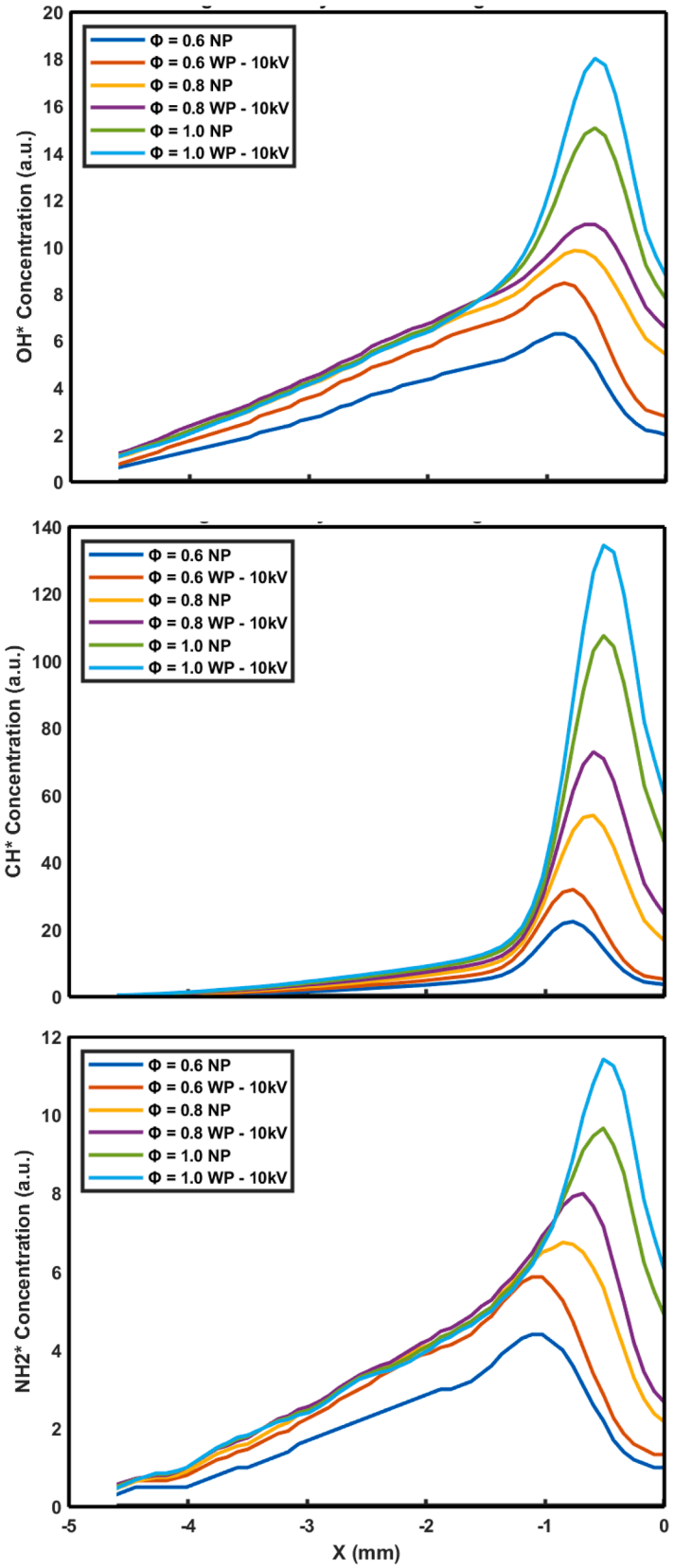

Fig. 5. Radical Species Signal Intensity at $y = 1$ .5mm.

application, the same cannot be said of the latter two radical species, with CH* showing minor variances in the image shape under the effects of plasma application, and NH_2* having a relatively significant alteration under the ns-DBD system. In order to better understand how the plasma actuation was able to modify the free radical concentration near the flame cone area, MATLAB image processing was applied to show the relationship between the average radical intensity near the flame cone area and the Average power applied to the plasma system, as a function of the RMS voltage. Fig. 6 shows the values for the OH* concentration, while Figs. 7 and 8 represent CH* and NH_2* respectively.

It can be seen from the graphs that while the OH* chemiluminescence signal follows no consistent trend win relation to the average power, both CH* and NH_2* follow a similar pattern wherein the first two instances are linearly increasing, then in between the 10 W and 30 W range, significantly increase before non-monotonically decreasing again. From the images, it can be seen just how much the influence of the ns-DBD plasma is on the radical concentration once a specific "trigger" or "critical value" is reached, as the normalized mean values significantly rise.

In order to better understand the explanation behind this phenomenon, Fig. 9 shows the relationship of the Input Voltage of the Nanosecond Pulse Generator to the (a) RMS Voltage and (b) Average Power. It can be seen that, across both cases, somewhere between the 4 kV and 6 kV input conditions a notable rise occurs for both the RMS Voltage and Average Power. This study presumes that is similar to the "critical" voltage found by Deng et al. [48], wherein the ionization process of the plasma begins in earnest as it transitions from an electric field to a plasma field, and brining with it all the other associated phenomena found in the literature.

The heightened signal intensity levels of NH_2* under plasma excitation, is assumed to be from its formation pathways outside of the oxidation of NH_3, as production of ground-state NH_2 in hydrocarbon/nitrous oxide combustion in the absence of ammonia involves the consumption of OH radicals, which agrees with the reduced amounts of local OH* at some levels of input energy observed in Fig. 6. Glarborg et al. [36] also discusses the role played by HCN to NH_2, which itself is an important intermediate in the Prompt NO pathway through R10 and R11. The pathway given below for the formation of NH_2 is highlighted by the intermediate HCN being a result of OH consumption [49] and NO formation [50].

$$CH_4 + OH \leftrightarrow CH_3 + H_2O \quad \text{(R26)}$$

$$N_2O + O \leftrightarrow 2NO \quad \text{(R27)}$$

$$CH_3 + NO \leftrightarrow HCN + H_2O \quad \text{(R28)}$$

$$HCN + OH \leftrightarrow HNCO + H \quad \text{(R29)}$$

$$HNCO + H \leftrightarrow NH_2 + CO \quad \text{(R30)}$$

Due to the excess amount of N_2O oxidizer present in fuel-lean conditions, it can be said that this promotes the consumption of OH radicals to produce excess NO and CO. Further investigations and analysis of the relationship between the increased concentration readings of CH* and NH_2* will be done after correlating the emission concentration values with the RMS Voltage and Average Power, and branching on from there.

4.2. Plasma effect on NO_x emissions

Despite the various benefits and potential possessed by NOFBX for aeronautical and aerospace applications, there is still a definite concern to be had when it comes to its emission characteristics. This is in part due to the N_2O oxidizer being a prime source of NO_x emissions, which possess a veritable slew of negative consequences on the environment and human health as a whole. This paper evaluates the effect of Nanosecond Pulsed Dielectric Barrier Discharge plasma (ns-DBD) on various emission behaviors of a premixed laminar $CH_4/N_2O/Ar$ flame. A Portable Syngas Analyzer by MRU Instruments was used to measure various emitted gases at the exit of the slot burner at a sampling distance of about 15cm. Based on the user manual, the flue gas analyzer possesses a detection limit of around 0.05 % or around 1 ppm with regards to the recorded concentration readings.

Fig. 10 shows the relative NO_x concentrations of the laminar $CH_4/N_2O/Ar$ flames under different equivalence ratios and different levels of ns-DBD average power. While the decrease of the NO_x emissions of the flames is observed as ϕ increased from 0.6 to 1.0 is consistent with previous works regarding NO_x and equivalence ratio [42], the results under plasma actuation were less than ideal.

Contrary to the initial goals of this study, NO_x emissions of the flames actually increased by a relatively significant margin under fuel-lean and slightly fuel-lean conditions, with a relatively negligible effect even at

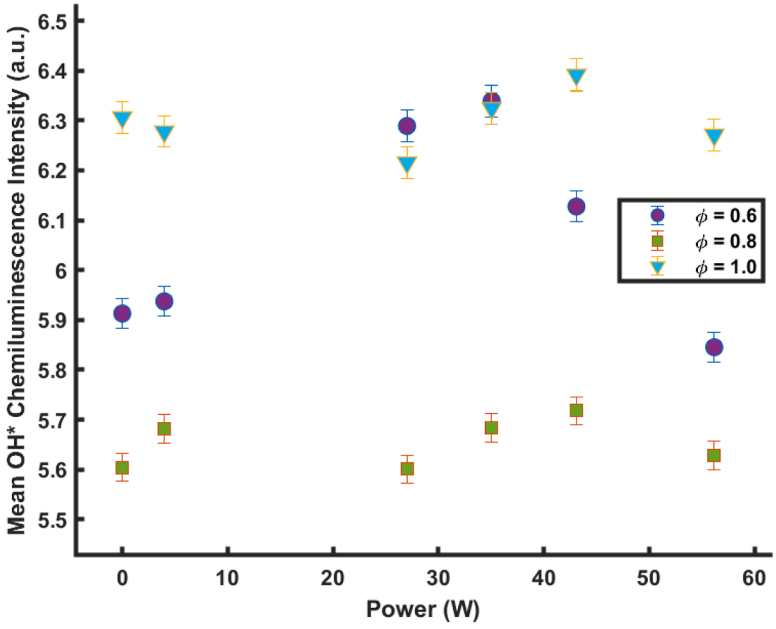

Fig. 6. Effect of Average Power on Average OH* Intensity.

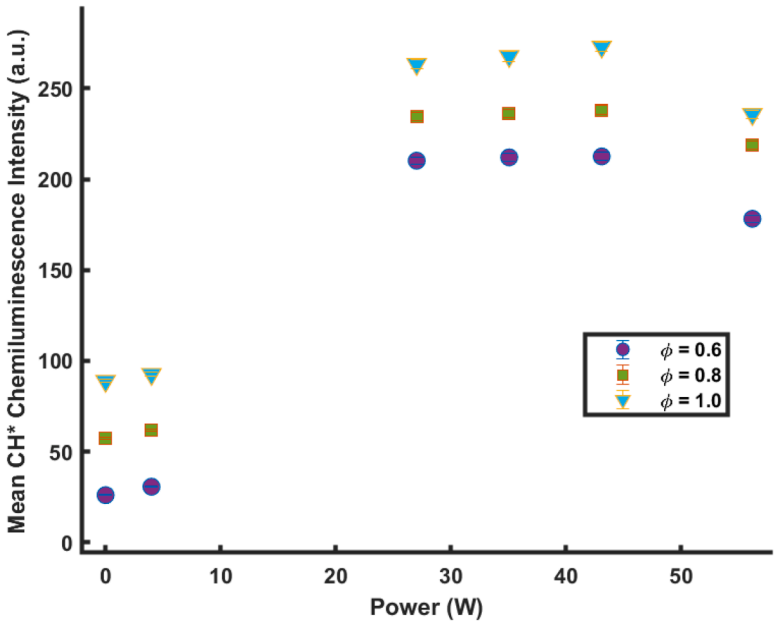

Fig. 7. Effect of Input Power on Average CH* Intensity.

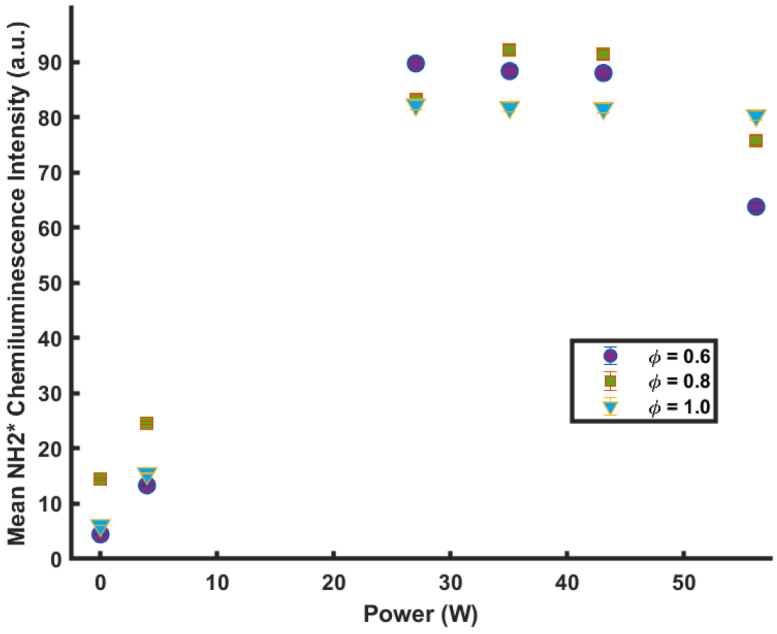

Fig. 8. Effect of Input Power on Average NH_2* Intensity.

stoichiometric conditions. At $\phi = 0.6$, the presence of ns-DBD plasma increased the relative NO_x emissions around an average of 25 %, with the highest increase being about 14,000 ppm to near 18,000 ppm, adjusted to 15 % O_2 content. For slightly fuel-lean conditions, the NO_x increase averaged at almost 15 %, while average emissions at stoichiometric conditions was merely around 1 %.

Based on the literature, plasma assistance has been shown to reduce NO_x emissions in flames with primarily or pure ammonia fuel due to the Thermal DeNO$_x$ mechanism [51], however when it comes to the application of PAC with fuels containing hydrocarbons or hydrogen in general, the effects of plasma assistance become a lot more inconsistent, as there have been studies showing both a decrease [30] and increase [27] in NO_x emissions as a result of plasma actuation. The difference between these results has been speculated to be due to the presence of hydrogen, which for the purposes of this study, comes from the methane fuel.

During the combustion process, CH_4 and N_2O break down into elementary radicals and species such as O, H, and OH. These are then responsible for NO production through the Thermal NO pathway as described previously in R1 to R5. Another way in which NOx is formed is through the Prompt NO pathway, highlighted by the attack of CH particles on molecular nitrogen as seen in R9. Since there is more visible increase of the CH* radical under plasma actuation, it is speculated that the influence of increased molecular oxygen produced by plasma by the decomposition of ozone [52] may be responsible for the bolstered Prompt NO formation. All of these may contribute to the heightened levels of NO_x at fuel-lean conditions, especially due to the oxidation of excess N_2O resulting in emissions containing O and NO.

While there is an increased amount of the NH_2* signal intensity

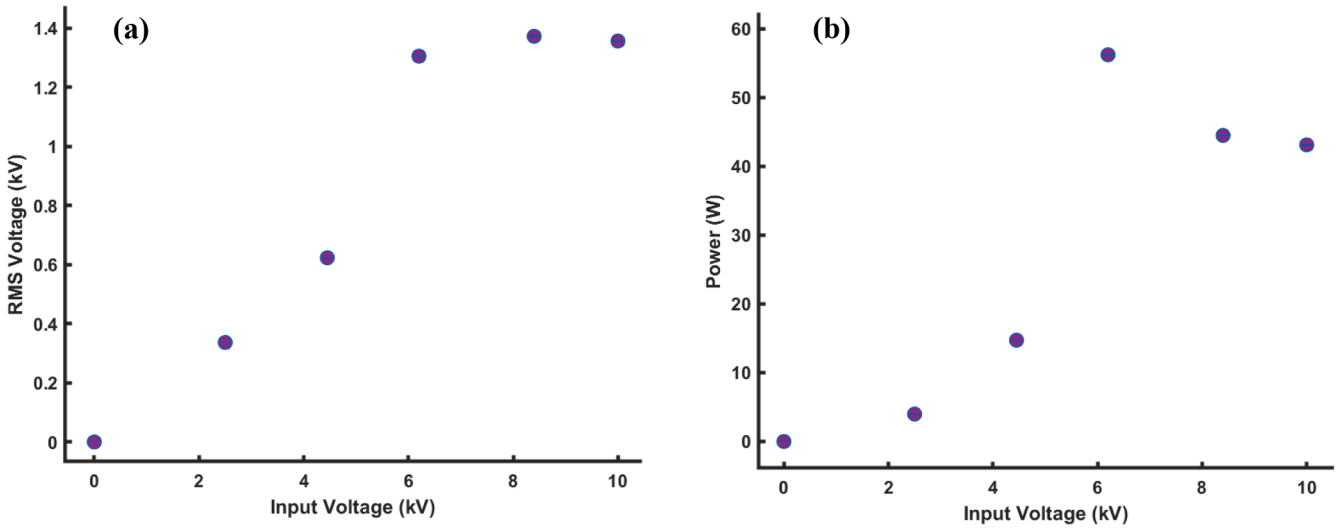

Fig. 9. ns-DBD Input Voltage plotted against **(a)** RMS Voltage and **(b)** Average Power.

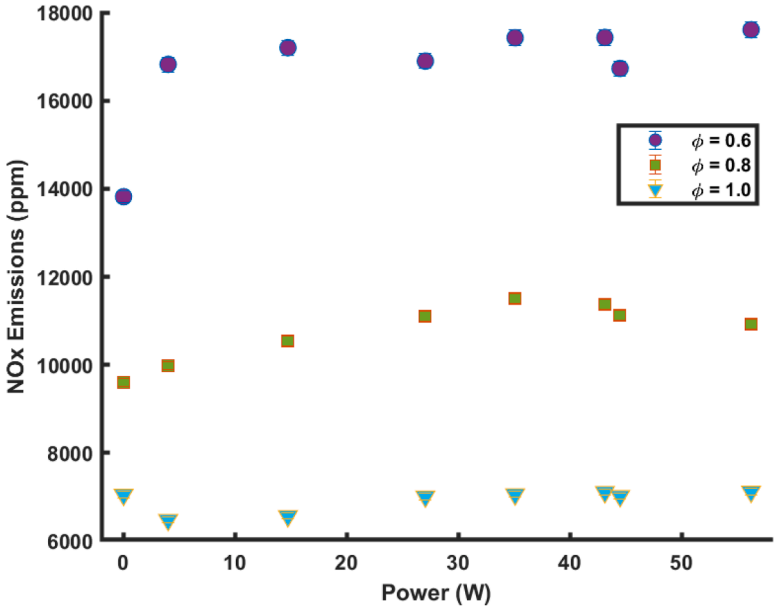

Fig. 10. Effect of ns-DBD plasma on NO_x emissions at different Input Power (W) and Equivalence Ratios.

observed in fuel-lean conditions, whose ground-state counterpart consumes NO and NO_2 as evidenced through R17 and R20, the increase in overall NO_x in the lean conditions is in line with previous work done by Ju et al. [27] wherein, in an Ammonia/Hydrogen/Air flame they inferred that hydrogen possesses a competitive relationship with regards to plasma when it comes to NO_x emission behaviors. It is recommended that future investigations observe if these results hold up to wider ranges as fuel-rich conditions were unable to be tested in this study. NH_2 in combustion configurations without ammonia fuel are formed by consumption of key species like OH and NO, such as in R26 and R29 respectively, which may be a point of interest in the future.

To further elucidate the relationship between PAC and NOx emissions, the recorded concentration values were plotted against the RMS Voltage in Fig. 11. Contrary to the graph showcasing emissions against average power, there is a much clearer observation to be had looking at the values on display. While it can be seen that for the values before the "critical" voltage are achieved, there is a stable trend of the emission characteristic values, however once the RMS voltage takes the transition to the plasma regime, the emission concentration readings approach similar values. This is, again, speculated to be caused by the transition to the plasma regime from the mere electric field regime, wherein the disconnect is due to the combustible mixture being ionized by the input energy from the ns-DBD pulse generator. While the trend when it comes to Power is non-monotonic, contrasting the results against RMS Voltage shows where exactly the clear separation occurs. Since this study contradicts previous research with regards to the effects of plasma actuation on fuel emissions, showing a non-monotonic increase rather than a decrease, it highlights the need for further investigation of plasma assistance in combustion and propulsion technologies promoting further development of sustainable propulsion mechanisms.

4.3. *Plasma effect on unburned hydrocarbons*

Unburned hydrocarbons (UHCs) like CH_4 present a clear and present danger to not only human society as smog which may cause a variety of different health issues, but also to the environment as greenhouse gases and local pollutants [53]. As such, different emission control mechanisms have been investigated towards reducing their concentrations,

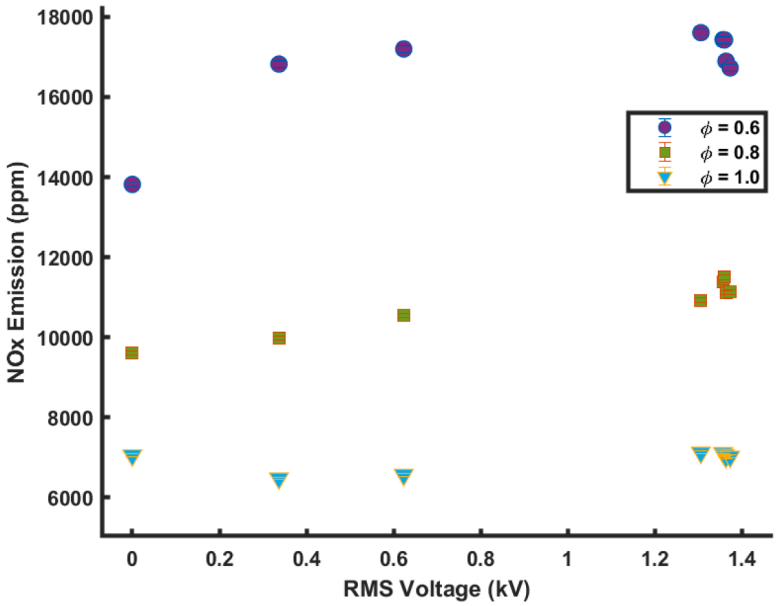

Fig. 11. Effect of ns-DBD plasma on NO_x emissions at different RMS Voltage (kV) and Equivalence Ratios.

especially when it comes to fuel combustion applications. Plasma assistance, for the most part, when it comes to UHC abatement have been in the form of internal and diesel engines [54].

Fig. 12 shows the effect of ns-DBD plasma on CH_4 emissions for different Input Power conditions and Equivalence Ratios for the CH_4/N_2O/Ar premixed laminar flame. It can be immediately observed that as both equivalence ratio and plasma power increase, the measured concentration of CH_4 drops drastically, although non-monotonically. Similar to the results found with NOx, Fig. 13 plots the emissions of CH_4 against the RMS Voltage, and much like before, there is a clearly visible trend before and after the critical value is reached, highlighting the disruptive capacity of PAC when it comes to the emissions of UHCs, due to the highly ionizing energy found. While in both cases the decreased in CH_4 emissions was non-monotonic due to the energy input, the results still show that PAC has the potential to greatly reduce the harmful effect of these unburned hydrocarbons.

Even at fuel-lean conditions, where combustion is expected to be incomplete due to the excess amount of N_2O oxidizer, UHC reduction averages greater than 50 %. At stoichiometric conditions, the total fuel conversion rate approaches almost 100 % which is indicative of the ability of PAC to enhance the overall combustion process. The literature refers to this phenomenon as "hydrocarbon cracking" [55], wherein plasma accelerates or enhances the pyrolysis and oxidation processes when it comes to hydrocarbons. This not only reduces them into smaller and simpler species, but has also been found to produce other radicals not easily generated otherwise.

The hydrocarbon cracking process when it comes to methane fuels, involves the breakdown or oxidation into smaller hydrocarbon compounds like CH_3, which consume NO such as in R28, and molecular H or H_2 which are highly reactive with other intermediates in the combustion process [56]. This also is in line with the chemiluminescence results showing an increase in OH* and NH_2* signals, as their ground state

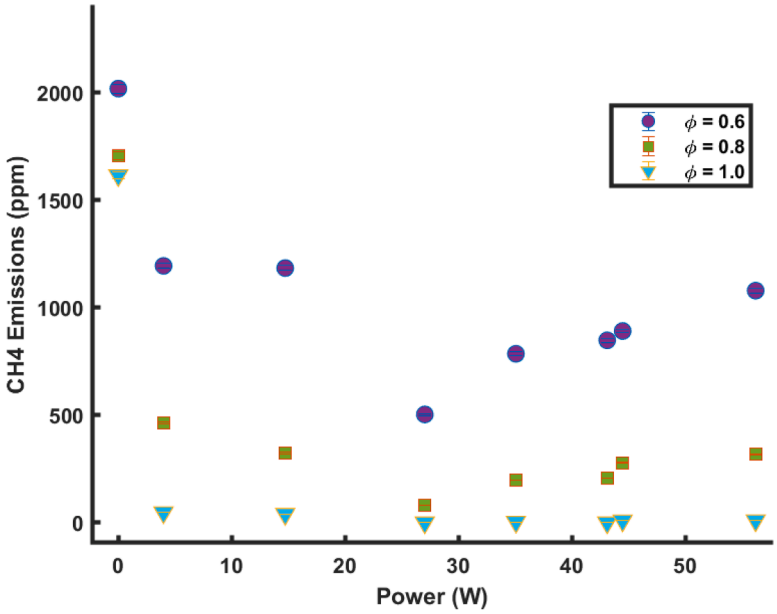

Fig. 12. Effect of ns-DBD plasma on CH_4 emissions at different Average Power (W) and Equivalence Ratios.

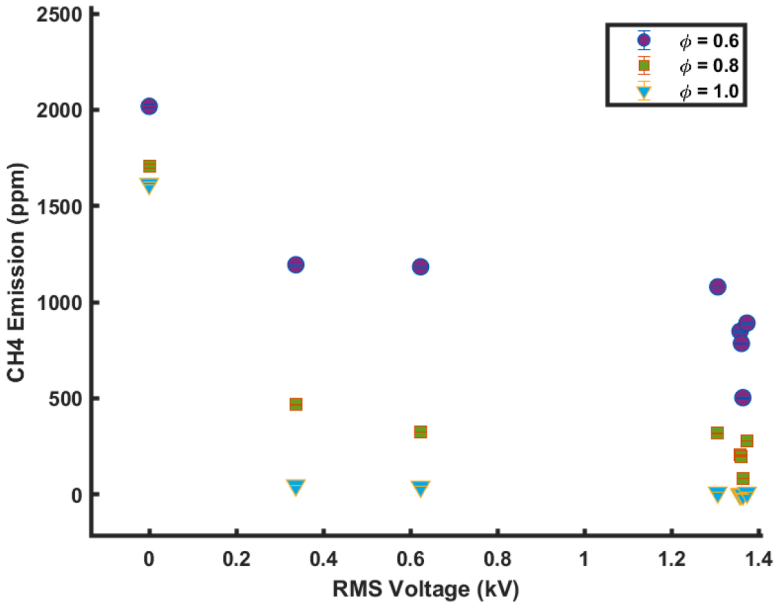

Fig. 13. Effect of ns-DBD plasma on CH_4 emissions at different RMS Voltage (kV) and Equivalence Ratios.

counterparts are just some of the key species produced by results of increased hydrocarbon cracking due to plasma effects. This occurrence may be caused by a variety of different plasma induced effects, which include charge exchange and electron impact excitation [20]. Some of these radical producing reactions involving methane and its byproducts are catalogued below, with the molecular CH and H being integral parts of various NO forming and consuming processes in the thermal combustion reaction.

$$CH_4 + e \leftrightarrow CH_4^+ + 2e \quad \text{(R31)}$$

$$CH_4^* + e \leftrightarrow CH_3 + H \quad \text{(R32)}$$

$$CH_4^* + e \leftrightarrow CH_2 + 2H \quad \text{(R33)}$$

$$CH_3^* + e \leftrightarrow CH_2 + H \quad \text{(R34)}$$

$$CH_2^* + e \leftrightarrow CH + H \quad \text{(R35)}$$

4.4. Plasma effect on CO_x

The most common Carbon Oxides, CO and CO_2, henceforth referred to as CO_x, are responsible for a wide variety of adverse effects on both human health and the environment, including but not limited to promoting the greenhouse effect and various cardiovascular diseases [57], which means that efforts to control or reduce their production during combustion processes is to be considered a worthwhile effort. As of late, PAC has been gaining great interest in the fields of carbon capture [58] and catalysis into more useful products so the literature on its effectiveness on CO_x is well understood. Nevertheless, the body of knowledge surrounding emissions of NOFBX as a fuel, especially considering ns-DBD is still lacking which highlights any future research into the topic as necessary.

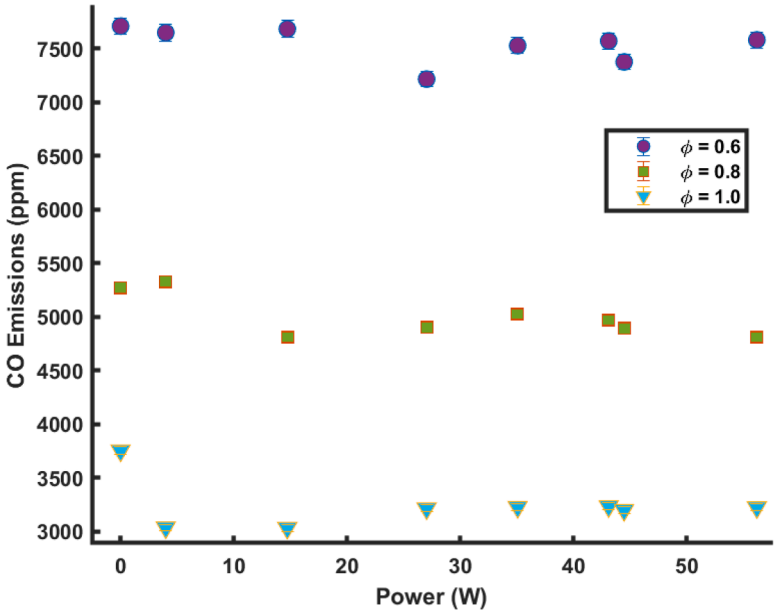

Fig. 14. Effect of ns-DBD plasma on CO emissions at different Average Power (W) and Equivalence Ratios.

Fig. 14 shows the effect of ns-DBD plasma on CO emissions for different Input Power conditions and Equivalence Ratios for the CH_4/N_2O/Ar premixed laminar flame. Compared to the effect of PAC on CH_4, CO is far less affected by the influence of PAC, as even in the RMS Voltage graphs seen in Fig. 15, there is only a slight non-monotonic decrease at the stoichiometric level, with little effect at fuel-lean before the critical value is reached and all the emission concentration readings bind together. Since Carbon Monoxide is a result of incomplete combustion and a lack of Oxygen, it was presumed that the molecular Oxygen previously discussed would be able to contribute to the reaction from the increased plasma energy input, but this was not the case.

While it is also true that CO emissions decrease as equivalence ratio increases, the effect of ns-DBD plasma also becomes more prominent with richer fuel concentrations. These two phenomena may influence one another as the increased presence of CH_4 fuel leads to the production of intermediate species which can help break down or consume CO. As Carbon Monoxide in it of itself is a result of incomplete combustion, it naturally follows that as combustion becomes more complete through plasma assistance, as evidenced by the UHC reduction, CO presence would also go down. This is further supported by the literature on the matter, as the most common CO consuming reaction is with OH [59], showcasing their inversely proportional relationship. Other CO reduction pathways involving plasma that have been investigated in previous studies include recombination and collision reactions [58] due to the heightened levels of electron temperature and density as a result of plasma actuation.

$$CO + OH \leftrightarrow CO_2 + H \quad \text{(R36)}$$

$$CO + O + M \leftrightarrow CO_2 + M \quad \text{(R37)}$$

$$CO + O_2 \leftrightarrow CO_2 + O \quad \text{(R38)}$$

$$CO + O^- \leftrightarrow CO_2 + e^- \quad \text{(R39)}$$

It can be seen that most of the CO consuming reactions listed result in CO_2, which according to Fig. 16 shows a trend similar to the effect of plasma on CH_4, but also unique in some ways. First, relating to Power, it can be seen that CO_2 without plasma assistance records the highest value at stoichiometric conditions. However, as plasma actuation increases, the stoichiometric readings takle a significant drop, ending up even lower than the fuel lean conditions, albeit in a non – monotonic pattern. This trend holds true even under the RMS Voltage conditions presented in Fig. 17, wherein even before the critical value is reached and the ionization process begins in earnest, the stoichiometric concentrations of CO_2 are already reduced below fuel-lean levels with just the electric field effect alone.

Past work attributes the effect of the increased ns-DBD intensity on the CO_2 emissions as a conversion effect through various process such as ionization, vibration excitation, and electron dissociation, all of which happen as a result of the increased energy introduced into the combustion system [58], however there are yet concerns with the energy efficiency of using PAC for CO_2 processing as to generate them it is usually non-renewable fossil fuels that are used. It can be seen in Fig. 16 there is a general trend to be seen that as input power increases, so too does the decrease in CO_2. The reactions below highlight the primary processes [60] involved in CO_2-plasma interactions. Despite CO_2 being the marker for more complete combustion and CO being the marker for incomplete combustion, both have been fond to decrease with the increasing equivalence ratio, or more complete combustion under plasma actuation. While CO_2 peaked at stoichiometric, plasma-free conditions, CO remains consistently high at fuel-lean conditions and showed only modest losses at stoichiometric under all plasma excitation levels. This phenomenon is speculated to be due to the interplay between their recombination and formation reactions highlighted in this section, wherein CO is converted into CO_2 and vice versa, with only the latter having a particularly sensitive and pronounced reaction to the increased plasma presences from the ns-DBD reactor.

$$e^- + CO_2 \rightarrow CO_2^+ + e^- + e^- \quad \text{(R40)}$$

$$e^- + CO_2 \leftrightarrow CO_{2vi} + e^- \quad \text{(R41)}$$

$$e^- + CO_2 \leftrightarrow CO_{2e_2} + e^- \quad \text{(R42)}$$

$$CO_2 + M \leftrightarrow CO + O + M \quad \text{(R43)}$$

$$CO_2 + O \leftrightarrow CO + O_2 \quad \text{(R44)}$$

R40 represents the principal ionization process, wherein the electrons induced by plasma interact with the ground-state CO_2, while R41 and R42 represent possible vibrational or electronic excitation of CO_2, depending on the energy levels which can vary due to power input and plasma type, with the subscripts referring to their specific excited states,

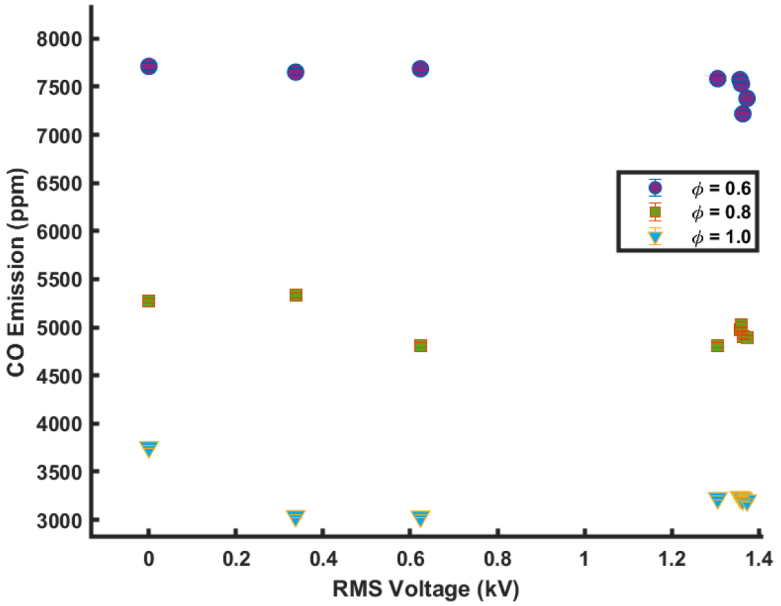

Fig. 15. Effect of ns-DBD plasma on CO emissions at different RMS Voltage (kV) and Equivalence Ratios.

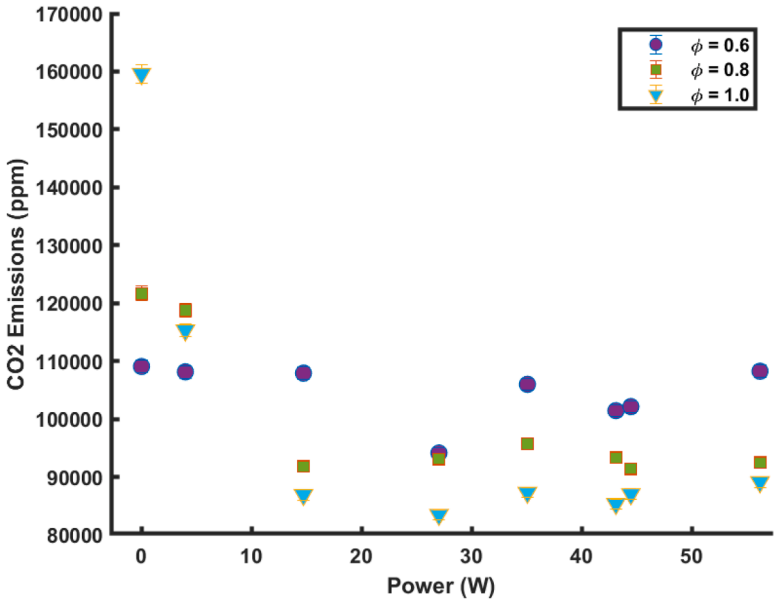

Fig. 16. Effect of ns-DBD plasma on CO_2 emissions at different Average Power (W) and Equivalence Ratios.

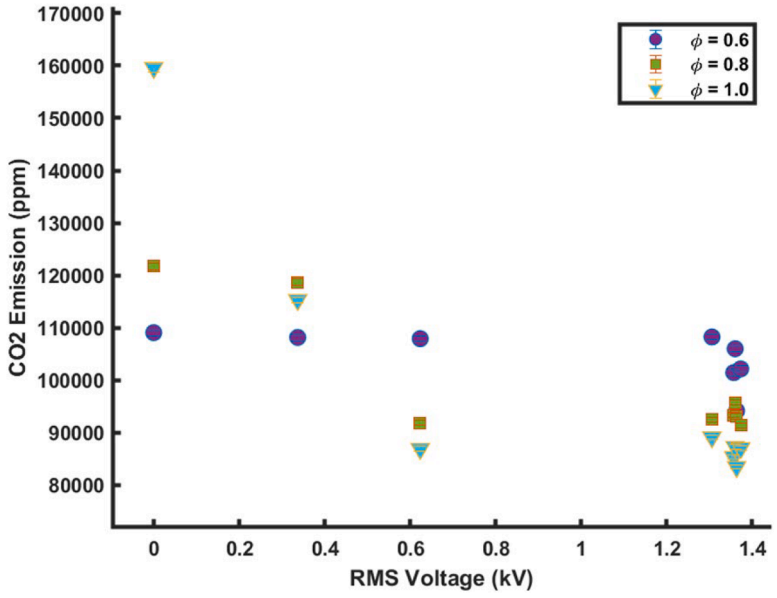

Fig. 17. Effect of ns-DBD plasma on CO_2 emissions at different RMS Voltage (kV) and Equivalence Ratios.

vi referring to vibrationally excited state and e_2 referring to electronically excited state. Lastly, R43 and R44 are representative of the dissociation effect of plasma wherein CO_2 is broken down into CO and radical/molecular oxygen. As seen from R36-R39 the interrelationship between quenching and formation of CO_x can take a variety of different forms, although more research has gone towards the reduction of CO_2 as it possesses a more immediate threat to human health and nature. Comparing the results found in Figs. 15. and 16. shows that when it comes to CO_x reduction by plasma in hydrocarbon/nitrous oxide flame configurations, CO_2 is both affected and reduced far more than CO, which may serve as a benchmark for future studies involving emission control. Additionally, since CO and CO_2 can represent the combustion efficiency, it was found that, at best, combustion efficiency was only improved by a factor of 3 %, which may be in part due to the fact that CO_2 was reduced far more than CO in (4).

5. Conclusion

Hydrocarbon/Nitrous Oxide fuel blends, typically called HyNOx or NOFBX, are being investigated as a potential propellant for aeronautic and aerospace applications, however there is still a great lack of research to be done, especially with regards to their emission characteristics, as the Nitrous Oxide oxidizer may be a source of the common and hazardous Nitrogen Oxide pollutants.

This study investigated the effect of varying levels of input power for an Nanosecond Pulsed Dielectric Barrier Discharge actuator to the emission characteristics of a $CH_4/N_2O/Ar$ premixed laminar flame. Plasma discharge was applied through a quartz slot burner and emission particle concentrations in PPM were taken for three different equivalence ratio cases. One fuel-lean at $\phi = 0.6$; another at slightly fuel-lean conditions at $\phi = 0.8$; and lastly at stoichiometric conditions where $\phi = 1.0$. Chemiluminescence imaging was used to measure and observe the

change in radical signal intensities under ns-DBD actuation of several key species involved in the combustion and emission formation behaviors of NOx. Additionally, flue gas analysis through a portable syngas analyzer was performed to measure, record, and quantify the overall plasma actuation effect. The main conclusions of this study are as follows:

1. Local signal intensity measurements of OH*, CH*, and NH_2* were found to increase in the primary flame cone area above the burner exit ($y = 1.5$ mm) in response to the presence of ns-DBD plasma actuation, however overall averaged spatial concentrations were observed to have varying degrees of sensitivity with regards to input power. Compared to the OH* signal, CH* and NH_2* signal were found to be much more sensitive to plasma excitation in the flame cone area. The existence of a "critical voltage value" is presumed to exist as the boundary between the electric field and the transition to the plasma field can be seen in the recorded values of the latter two radicals when plotted against the RMS Voltage values of the ns-DBD Pulse Generator.
2. Under the effects of ns-DBD plasma, relative NO_x emissions were found to increase by almost 25 % on average in the fuel-lean condition. This was attributed to the PAC promoting the Prompt NO formation pathway, due to the increased amount of N_2O oxidizer resulting in the amplified CH* signal intensity measured across all conditions. As equivalence ratio increased, the NO_x increase due to plasma presence also subsided. It is speculated that the increase in molecular Oxygen due to plasma actuation resulted in a more abundant CH*concentration, which led to the NO promotion rather than reduction. NH_2* despite also increasing with plasma power, was unable to result in meaningful NOx abatement.
3. Increasing plasma intensity from input power was found to be induce a relatively non-monotonic reduction in the emission concentrations of CH_4 and CO_2. These effects are believed to be caused by kinetic enhancement via plasma and the generation of important key intermediate species for the promotion of oxidation and consumption reactions. This, alongside phenomena such as hydrocarbon cracking and electron impact excitation, are able to have a significant impact on combustion product emissions. However, a simultaneous reduction of these prior pollutants and NO_x has yet to be achieved, suggesting that there may be a competitive relationship to their formation in hydrocarbon/nitrous oxide flame configurations.

Although the initial objective of being able to reduce NOx concentrations through the use of ns-DBD plasma was not met, this study still provides significant insight towards the fields of "green fuel" propulsion and plasma assisted combustion in general. Since the results contradict prior assumptions regarding the ability of plasma actuation to reduce emissions, the need for deeper and more thorough investigation behind the coupling mechanics of plasma-flame interactions is stressed. By inspiring future studies to delineate the exact interplay mechanics between emissions from combustion and plasma, the development of sustainable propulsion mechanisms and plasma systems is advanced.

5.1. Limitations and recommendations

Unfortunately, there are some key limitations of the study that must be acknowledged, alongside recommendations for future research. It is suggested that future researchers, when investigate the interconnected mechanics of flame-plasma interactions, also investigate their behavior at fuel-rich conditions, which was unable to be observed in this study due to safety concerns with the quartz slot burner and electrode setup. Additionally, different types of plasma may have varying effects on different types of burner configurations and it is suggested that outside of one fuel type and plasma type, future researchers hoping to investigate this topic make use of the wide spectrum of plasma data to draw their conclusions based on the existing body of knowledge. Due to the great effort needed when it comes to wholly investigating fuel emissions under plasma assistance, other green propellants are suggested to be subjected to plasma influence, as they may yet result in more comprehensive reduction capacities against testing only a single green fuel.

Funding

This study was supported by the National Science and Technology Council of Taiwan (NSTC 112-2923-E-006-002-MY3; NSTC 112-2628-E-006-00112-2628-E-006-005-MY35-MY3; NSTC 113-2223-E-006-010E-006-010) and the National Center for Research and Development in Poland (POLTAJ10/2022/49/MethaHydrAmmon).

CRediT authorship contribution statement

Boj N. Villanueva: Writing – original draft, Software, Investigation, Formal analysis, Data curation. **Po-Hung Lin:** Validation, Investigation, Formal analysis, Conceptualization. **Yueh-Heng Li:** Validation, Supervision, Resources, Project administration, Methodology, Funding acquisition. **Jaime P. Honra:** Validation, Supervision, Funding acquisition.

Declaration of competing interest

All authors declared that: (i) no support, financial or otherwise, has been received from any organization that may have an interest in the submitted work; and (ii) there are no other relationships or activities that could appear to have influenced the submitted work.

Acknowledgments

This study was financially supported by the National Science and Technology Council of Taiwan (NSTC 112-2923-E-006-002-MY3; NSTC 112-2628-E-006-005112-2628-E-006-005-MY3; NSTC 113-2223-E-006-010-MY3; NSTC 113-2223-E-006-010) and the National Center for Research and Development in Poland (POLTAJ10/2022/49/MethaHydrAmmon).

Data availability

Data will be made available on request.

References

[1] S. Carlotti, F. Maggi, Evaluating new liquid storable bipropellants: safety and performance assessments, Aerospace 9 (10) (2022) 561.
[2] H.V.N. Nguyen, J.A. Chenoweth, V.S. Bebarta, T.E. Albertson, C.D. Nowadly, The toxicity, pathophysiology, and treatment of acute hydrazine propellant exposure: a systematic review, Mil. Med. 186 (3–4) (2021) e319–e326.
[3] A. Sarritzu, A. Pasini, F. Merz, L. Werling, F. Lauck, Experimental investigation of combustion performance of a green hypergolic bipropellant based on hydrogen peroxide, Acta Astronaut. 219 (March) (2024) 278–290.
[4] Y.H. Li, B.C Chuang, P.H. Li, J. Lasek, Effects of ammonia on combustion of coal in premixed methane-air flames, Fuel 350 (2023) 128825.
[5] A. Okninski, et al., Development of green storable hybrid rocket propulsion technology using 98% hydrogen peroxide as oxidizer, Aerospace 8 (9) (2021) 234.
[6] Y.H. Li, J.W. Liang, H.J. Lin, Development of laminar burning velocity measurement system in premixed flames with hydrogen-content syngas or strong oxidizer conditions in a slot burner, Case Stud. Therm. Eng. 35 (2022) 102162.
[7] Y.H. Li, S.K. Reddy, C.H. Chen, Effects of the nitrous oxide decomposition reaction on soot precursors in nitrous oxide/ethylene diffusion flames, Energy 235 (2021) 121364.
[8] L. Werling, et al., Nitrous oxide fuels blends: research on premixed monopropellants at the german aerospace center (DLR) since 2014, AIAA Propuls. Energy 2020 Forum (2020) 1–21.
[9] Y. Li, S. Xu, Y. Liu, J. Cui, F. Xu, Flame propagation characteristics and gas-phase oxidation of nitrous oxide and propane, Case Stud. Therm. Eng. 59 (May) (2024) 104574.
[10] Y.H. Li, C.H. Hsu, P.H. Lin, C.H. Chen, Thermal effect and oxygen-enriched effect of N_2O decomposition on soot formation in ethylene diffusion flames, Fuel 329 (July) (2022) 125430.

[11] U. Asghar, et al., Review on the progress in emission control technologies for the abatement of CO_2, SO_x and NO_x from fuel combustion, J. Environ. Chem. Eng. 9 (5) (2021) 106064.
[12] S. Bhowmick, A. Badiwal, K.T. Shenoy, Removal of NO_x using ozone injection and subsequent absorption in water, Chem. Eng. J. Adv. 15 (x) (2023) 100511.
[13] J. Sajedifar, S. Bagher, H. Asilian, A. Khavanin, Design and implementation of a cost-effective, safe, and precise lean-rich generating system for the evaluation of NOx storage reduction catalysts : performance analysis, statistical modeling, and multiple response optimization – A guideline for futu, Result. Eng. 25 (November 2024) (2025) 103621.
[14] Y. Zhang, T. Li, X. Wei, Influence of non-thermal plasma and electric field on non-premixed methane flame, Therm. Sci. Eng. Prog. 47 (December 2023) (2024) 102366.
[15] S. Huang, Z. Zhang, H. Song, Y. Wu, Y. Li, A novel way to enhance the spark plasma-assisted ignition for an aero-engine under low pressure, Appl. Sci. 8 (9) (2018) 1533.
[16] Y. Ju, W. Sun, Plasma assisted combustion: dynamics and chemistry, Prog. Energy Combust. Sci. 48 (2015) 21–83.
[17] J.A.T. Gray, D.A. Lacoste, Enhancement of the transition to detonation of a turbulent hydrogen–air flame by nanosecond repetitively pulsed plasma discharges, Combust. Flame 199 (2019) 258–266.
[18] Y. Tian, et al., Combustion enhancement in a model scramjet by a simple pin-to-pin AC arc plasma, Proc. Combust. Inst. 40 (1–4) (2024) 105259.
[19] J. Sun, W. Cui, Y. Tang, C. Kong, S. Li, Inlet pulsation-induced extinction and plasma-assisted stabilization of premixed swirl flames, Fuel 328 (July) (2022) 125372.
[20] Y. Tang, J. Zhuo, W. Cui, S. Li, Q. Yao, Enhancing ignition and inhibiting extinction of methane diffusion flame by in situ fuel processing using dielectric-barrier-discharge plasma, Fuel Process. Technol. 194 (2019) 106128.
[21] R. Feng, et al., Suppression of combustion mode transitions in a hydrogen-fueled scramjet combustor by a multi-channel gliding arc plasma, Combust. Flame 237 (2022) 111843.
[22] O. Molchanov, K. Krpec, J. Horak, L. Kubonova, F. Hopan, J. Rysavý, Combined control of PM and NO_x emissions from small-scale combustions by electrostatic precipitation, Results Eng 24 (2024) 103255.
[23] R. Ju, et al., Stability and emission characteristics of ammonia/air premixed swirling flames with rotating gliding arc discharge plasma, Energy 277 (June 2022) (2023) 127649.
[24] R. Paulauskas, E. Bykov, K. Zakarauskas, N. Striūgas, R. Skvorčinskienė, Effects of plasma-produced ozone on flame chemiluminescence and pollutant emissions of biogas with different CO_2 content, Plasma Chem. Plasma Process. 43 (4) (2023) 831–847.
[25] M. Li, Z. Wang, R. Xu, X. Zhang, Z. Chen, Q. Wang, Advances in plasma-assisted ignition and combustion for combustors of aerospace engines, Aerosp. Sci. Technol. 117 (2021) 106952.
[26] Y.H. Li, C.H. Chen, M. Ilbas, Effect of diluent addition on combustion characteristics of methane /nitrous oxide inverse tri-coflow diffusion flames, Combust. Sci. Technol. 194 (10) (2022) 1973–1993.
[27] R. Ju, et al., Experimental study on burning velocity, structure, and NOx emission of premixed laminar and swirl NH_3/H_2/air flames assisted by non-thermal plasma, Appl. Energy Combust. Sci. 14 (January) (2023) 100149.
[28] L. Werling, Y. Jooß, M. Wenzel, H. Ciezki, S. Schlechtriem, A premixed green propellant consisting of N_2O and C_2H_4: experimental analysis of quenching diameters to design flashback arresters, Int. J. Energ. Mater. Chem. Propuls. 17 (3) (2018) 241–262.
[29] Y. Tang, J. Zhuo, W. Cui, S. Li, Q. Yao, Non-premixed flame dynamics excited by flow fluctuations generated from dielectric-barrier-discharge plasma, Combust. Flame 204 (2019) 58–67.
[30] J. Sun, Q. Huang, Y. Tang, S. Li, Stabilization and emission characteristics of gliding arc-assisted NH3/CH4/air premixed flames in a swirl combustor, Energy Fuel. 36 (15) (2022) 8520–8527.
[31] X. Tian, J. Yang, Y. Gong, Q. Guo, X. Wang, G. Yu, Experimental study on OH*, CH*, and CO_2* chemiluminescence diagnosis of CH_4/O_2 Diffusion flame with CO_2-diluted fuel, ACS Omega 7 (45) (2022) 41137–41146.
[32] M.M. Kamal, Two-line (CH*/CO_2*) chemiluminescence technique for equivalence ratio mapping in turbulent stratified flames, Energy 192 (2020) 116485.
[33] H.H. Chen, C.Y. Wu, Experimental investigation of the plasma-assisted spray combustion of methanol/water mixtures, Fuel 363 (January) (2024) 130972.
[34] C.R. Mulvihill, E.L. Petersen, OH* chemiluminescence in the H_2-NO_2 and H_2-N_2O systems, Combust. Flame 213 (2) (2020) 291–301.
[35] M. Zhao, D. Buttsworth, R. Choudhury, Experimental and numerical study of OH * chemiluminescence in hydrogen diffusion flame, Combust. Flame 197 (2018) 369–377.
[36] P. Glarborg, J.A. Miller, B. Ruscic, S.J. Klippenstein, Modeling nitrogen chemistry in combustion, Prog. Energy Combust. Sci. 67 (2018) 31–68.
[37] Y. Liu, J. Tan, M. Wan, L. Zhang, X. Yao, Quantitative measurement of OH* and CH* chemiluminescence in jet diffusion flames, ACS Omega 5 (26) (2020) 15922–15930.
[38] Y. Tang, D. Xie, C. Wei, B. Huang, B. Shi, N. Wang, Effect of microsecond repetitively pulsed discharges on lean blow-off limit and emission of rapidly-mixed ammonia/air swirling flames, Appl. Energy Combust. Sci. 14 (May) (2023) 100140.
[39] L. Cheng, N. Barleon, B. Cuenot, O. Vermorel, A. Bourdon, Plasma assisted combustion of methane-air mixtures: validation and reduction, Combust. Flame 240 (2022) 111990.
[40] R.A. Varella, J.C. Sagás, C.A. Martins, Effects of plasma assisted combustion on pollutant emissions of a premixed flame of natural gas and air, Fuel 184 (2016) 269–276.
[41] S.D. E, M. Ebrahimi, S. Gholamhosein, Experimental investigation, modeling and prediction of transition from uniform discharge to filamentary discharge in DBD plasma actuators using artificial neural network, Appl. Therm. Eng. 129 (2018) 50–61.
[42] Y. Liu, J. Tan, Z. Gao, T. Wang, M. Wan, Experimental investigation of chemiluminescence and NOx emission characteristics in a lean premixed dual-swirl flame, Case Stud. Therm. Eng. 28 (November) (2021) 101653.
[43] N. Garan, S. Dybe, C. Oliver, N. Djordjevic, Consistent emission correction factors applicable to novel energy carriers and conversion concepts, Fuel 341 (May 2022) (2023) 127658.
[44] L. Xia, G. Zhang, L. Liu, B. Li, M. Zhan, P. Kong, Atmospheric CO_2 and CO at Jingdezhen station in central China: understanding the regional transport and combustion efficiency, Atmos. Environ. 222 (July 2019) (2020) 117104.
[45] R. Kowalik, Influence of initial temperature on laminar burning velocity in hydrogen-air mixtures as potential for green energy carrier, Int. Commun. Heat Mass Transfer 146 (2023) 106861.
[46] C. Chen, et al., Experimental and kinetic modeling study of laminar burning velocity enhancement by ozone additive in NH_3+O_2+N_2 and NH_3+CH_4/C_2H_6/C_3H_8+air flames, Proc. Combust. Inst. 39 (4) (2023) 4237–4246.
[47] L. Xie, et al., A novel dielectric barrier discharge ozone generator with excellent microdischarge temperature behavior, Appl. Therm. Eng. 250 (February) (2024) 123453.
[48] K. Deng, S. Zhao, C. Xue, J. Hu, Y. Zhong, Y. Zhong, Combustion instability of swirl premixed flame with dielectric barrier discharge plasma, Processes 9 (8) (2021).
[49] Y. Shang, J. Shi, H. Ning, R. Zhang, H. Wang, S. Luo, Ignition delay time measurements and kinetic modeling of CH_4 initiated by CH_3NO_2, Fuel 243 (February) (2019) 288–297.
[50] N. Lamoureux, L. Gasnot, P. Desgroux, Quantitative NH measurements by using laser-based diagnostics in low-pressure flames, Proc. Combust. Inst. 37 (2) (2019) 1313–1320.
[51] Y. Tang, D. Xie, B. Shi, N. Wang, S. Li, Flammability enhancement of swirling ammonia/air combustion using AC powered gliding arc discharges, Fuel 313 (November 2021) (2022) 122674.
[52] W. Sun, X. Gao, B. Wu, T. Ombrello, The effect of ozone addition on combustion: kinetics and dynamics, Prog. Energy Combust. Sci. 73 (2019) 1–25.
[53] F. Leach, G. Kalghatgi, R. Stone, P. Miles, The scope for improving the efficiency and environmental impact of internal combustion engines, Transp. Eng. 1 (2020) 100005.
[54] M. Hsueh, et al., An analysis of exhaust emission of the internal combustion engine treated by the non-thermal plasma, Molecules 25 (41) (2020) 1–20.
[55] Y. Tang, Q. Yao, J. Zhuo, S. Li, Plasma-assisted pyrolysis and ignition of pre-vaporized n-heptane, iso-octane and n-decane, Fuel 289 (November 2020) (2021) 119899.
[56] Z. Fan, et al., COx-free co-cracking of n-decane and CH_4 to hydrogen and acetylene using pulsed spark plasma, Chem. Eng. J. 436 (January) (2022) 135190.
[57] H. Liu, Z. Li, Y. Yang, G. Miao, Relationship between temperature rise characteristics and the emission of carbon oxides during the spontaneous combustion latency of coal, J. Clean. Prod. 420 (August) (2023) 138380.
[58] M.Y. Ong, S. Nomanbhay, F. Kusumo, P.L. Show, Application of microwave plasma technology to convert carbon dioxide (CO_2) into high value products: a review, J. Clean. Prod. 336 (2022) 130447.
[59] A. Ghabi, et al., Effects of pulsed gliding arc plasma on non-premixed CH_4/CO_2– air flame stability, Therm. Sci. Eng. Prog. 40 (2023) 101764.
[60] Y. Qin, G. Niu, X. Wang, D. Luo, Y. Duan, Status of CO_2 conversion using microwave plasma, J. CO2 Util. 28 (September) (2018) 283–291.